AMERICAN SOCIETY FOR MICROBIOLOGY | Molecular and Cellular Biology

Hepatic Overexpression of CD36 Improves Glycogen Homeostasis and Attenuates High-Fat Diet-Induced Hepatic Steatosis and Insulin Resistance

Wojciech G. Garbacz,[a] Peipei Lu,[a] Tricia M. Miller,[b] Samuel M. Poloyac,[b] Nicholas S. Eyre,[c] Graham Mayrhofer,[c] Meishu Xu,[a] Songrong Ren,[a] Wen Xie[a,d]

Center for Pharmacogenetics and Department of Pharmaceutical Sciences, University of Pittsburgh, Pittsburgh, Pennsylvania, USA[a]; Department of Pharmaceutical Sciences, University of Pittsburgh, Pittsburgh, Pennsylvania, USA[b]; School of Biological Sciences, University of Adelaide, Adelaide, Australia[c]; Department of Pharmacology and Chemical Biology, University of Pittsburgh, Pittsburgh, Pennsylvania, USA[d]

The common complications in obesity and type 2 diabetes include hepatic steatosis and disruption of glucose-glycogen homeostasis, leading to hyperglycemia. Fatty acid translocase (FAT/CD36), whose expression is inducible in obesity, is known for its function in fatty acid uptake. Previous work by us and others suggested that CD36 plays an important role in hepatic lipid homeostasis, but the results have been conflicting and the mechanisms were not well understood. In this study, by using CD36-overexpressing transgenic (CD36Tg) mice, we uncovered a surprising function of CD36 in regulating glycogen homeostasis. Overexpression of CD36 promoted glycogen synthesis, and as a result, CD36Tg mice were protected from fasting hypoglycemia. When challenged with a high-fat diet (HFD), CD36Tg mice showed unexpected attenuation of hepatic steatosis, increased very low-density lipoprotein (VLDL) secretion, and improved glucose tolerance and insulin sensitivity. The HFD-fed CD36Tg mice also showed decreased levels of proinflammatory hepatic prostaglandins and 20-hydroxyeicosatetraenoic acid (20-HETE), a potent vasoconstrictive and proinflammatory arachidonic acid metabolite. We propose that CD36 functions as a protective metabolic sensor in the liver under lipid overload and metabolic stress. CD36 may be explored as a valuable therapeutic target for the management of metabolic syndrome.

Individuals with metabolic syndrome or type 2 diabetes are susceptible to nonalcoholic fatty liver disease (1) and disruption of hepatic glucose and glycogen homeostasis (2). Hepatic steatosis is defined as an excess accumulation of fat in hepatocytes. Previous reports suggested that fatty acid translocase (FAT/CD36) plays an important role in hepatic lipid homeostasis (3–6). CD36 is a multiligand class B scavenger receptor with high affinity for lipids and lipid-containing ligands. CD36 is known for its lipid uptake function in macrophages, skeletal muscle, and the heart. However, the role of CD36 in hepatic lipid metabolism is still not well understood, and the available evidence is often conflicting, partly due to the lack of a reliable *in vivo* liver-specific gain-of-function model to specifically evaluate the function of CD36 in the liver.

The basal expression of CD36 in the liver is low; however, it is highly inducible by a high-fat diet (HFD) (3). The hepatic expression of CD36 is under the transcriptional control of the nuclear receptors: liver X receptor (LXR), pregnane X receptor (PXR), peroxisome proliferator-activated receptors (PPARs), and the aryl hydrocarbon receptor (AhR) (4). Some studies have suggested that hepatic CD36, by functioning as a fatty acid transporter, has a role in the pathogenesis of hepatic steatosis (3), obesity (7, 8), and age-related hepatic steatosis (5). Furthermore, we and others reported that induction of CD36 was a common factor in fatty liver following the activation of LXR and PXR (6, 9). On the other hand, recent reports suggested that CD36 signaling might actually be beneficial in preventing fatty liver by promoting the formation and secretion of lipoprotein particles (10). It is conceivable that an *in vivo* model in which CD36 expression can be temporally and liver-specifically regulated will help to establish the function of CD36 in hepatic lipid metabolism and help to explain the discrepancies arising from earlier studies.

With CD36 emerging as a key player or even perceived as a causative factor in fatty liver and the associated metabolic syndrome, we hypothesize that CD36 may play an important role in energy metabolism in the liver, including the homeostasis of glycogen, which is known to be disrupted in diabetes and to contribute to the manifestation of dysglycemia (11–13). Glycogen is formed in the liver primarily in the postprandial high blood glucose state. The three key enzymes that are involved in hepatic glycogen turnover are glycogenin, glycogen synthase (GS), and glycogen phosphorylase (GP). Glycogenin initiates glycogen synthesis, whereas GS catalyzes the elongation of glycogen chains. GP catalyzes the breakdown of glycogen. GS and GP are enzymatically activated by dephosphorylation and phosphorylation, respectively. The activities of these enzymes are also subject to allosteric regulation (14). The phosphorylation of GP is catalyzed by several upstream kinases, such as glycogen synthase kinase 3β (GSK3β) and AMP-activated protein kinase (AMPK), whereas the dephosphorylation of GS is facilitated by protein phosphatase 1 (PP1) coupled with the glycogen-targeting regulatory subunits (15).

In diabetes and obesity, metabolism of glycogen in the liver is

Received 7 March 2016 **Returned for modification** 29 March 2016
Accepted 10 August 2016

Accepted manuscript posted online 15 August 2016

Citation Garbacz WG, Lu P, Miller TM, Poloyac SM, Eyre NS, Mayrhofer G, Xu M, Ren S, Xie W. 2016. Hepatic overexpression of CD36 improves glycogen homeostasis and attenuates high-fat diet-induced hepatic steatosis and insulin resistance. Mol Cell Biol 36:2715–2727. doi:10.1128/MCB.00138-16.

Address correspondence to Wen Xie, wex6@pitt.edu.

affected when triglyceride accumulation reaches levels that manifest pathologically as fatty liver (12, 16). GS activity often becomes dysregulated in steatosis, exacerbating the already existing dysglycemia (12, 17, 18). Recent reports have shown that hepatic overexpression of the G-regulatory subunits of PP1 increased hepatic glycogen accumulation, protected mice from fasting hypoglycemia, and accelerated postprandial blood glucose clearance in mice fed a chow diet or an HFD or in rats with streptozotocin-induced diabetes (15, 19, 20). Given the potential effect of CD36 on steatosis and the link between the homeostasis of glycogen and triglyceride, it is unclear whether CD36 has a direct effect on the homeostasis of glycogen, especially when the animals are under metabolic stress.

In this study, we uncovered a surprising function of CD36 in regulating glycogen homeostasis. Overexpression of CD36 in transgenic mice promoted glycogen synthesis, and as a result, CD36-overexpressing transgenic (CD36Tg) mice were protected from fasting hypoglycemia. We also showed that the CD36Tg mice were protected from HFD-induced hepatic steatosis and type 2 diabetes.

MATERIALS AND METHODS

Mice. To generate the tetracycline (Tet)-inducible "Tet-off" tetracycline response element (TetRE)-CD36/FABP-tTA transgenic mice, a tetracycline transactivator (tTA)-responsive TetRE-CD36 expression construct was assembled, consisting of the P_{tight} Tet-responsive promoter (from pTRE-Tight; Clontech), rat CD36 cDNA, simian virus 40 (SV40) poly(A) signal, *loxP*-flanked murine phosphoglycerate kinase gene (*Pgk*) promoter, neomycin resistance gene (*neo*^{r}) cDNA, SV40 poly(A) signal, and a 3′ splice donor sequence flanked by *loxP*. To generate a gene-targeting construct, the above-described expression construct was inserted between 5′ and 3′ homology arms from the murine *ROSA26* locus. C57BL/6 Bruce4 embryonic stem cells were subjected to gene targeting by Ozgene (Bentley, Australia), and a single line of TetRE-CD36 knock-in/transgenic mice carrying a single copy of the expression construct targeted to the *ROSA26* locus were identified. The TetRE-CD36 mice were then crossed with the hepatocyte-specific LAP-tTA transgenic mice expressing tTA under the control of the LAP (C/EBPβ) gene promoter (21) to generate TetRE-CD36/LAP-tTA double-transgenic mice. The CD36Tg mice and the age- and sex-matched wild-type (WT) control mice were in the C56BL/6 background. LAP-tTA transgenic mice [strain B6.Cg-Tg(Cebpb-tTA)5Bjd/] in the C56BL/6 background were purchased from the Jackson Laboratory.

Fasting of animals. WT and CD36Tg mice maintained on a normal chow diet were subjected to 0 h, 6 h, and 16 h of fasting to examine the dynamics of the hepatic glycogen content. Ten-week-old mice were used for this experiment to ensure the mice had sufficient body weight and size for the 16-h fast.

Treatment with an HFD and Dox. WT and CD36Tg mice were subjected to HFD feeding (60% calories from fat) starting at 6 to 7 weeks of age and fed *ad libitum* for 13 weeks. When necessary, the CD36Tg mice were treated with doxycycline (Dox) (CD36Tg plus Dox) by supplementing their drinking water with Dox at a concentration of 1 mg/liter.

GTT, ITT, and euglycemic-hyperinsulinemic clamp. Glucose tolerance tests (GTT) were performed on HFD-fed, 16-h-fasted mice with an intraperitoneal (i.p.) injection of D-glucose at 1 to 2 g/kg body weight. An insulin tolerance test (ITT) was performed on HFD-fed, 6-h-fasted mice with an intraperitoneal injection of insulin at 0.75 unit/kg body weight, as we have previously described (22). Euglycemic-hyperinsulinemic clamps were performed on HFD-fed 16-h-fasted mice, as we have previously described (23). The mice were constantly infused with [^{3}H]glucose at 0.05 μCi/min through a right jugular vein catheter in the basal state. In the clamp state, mice were infused with a primed dose of human insulin (from Novo Nordisk, Princeton, NJ) at 300 mU/kg body weight, followed by a constant insulin infusion at 2.5 mU/kg/min. [^{3}H]glucose was infused at 0.1 μCi/min. At the same time, 20% glucose was infused at a variable rate to maintain a blood glucose range between 120 and 140 mg/dl. Blood glucose levels were monitored every 10 min. Twenty microliters of blood was sampled at the end of the basal state and the clamp state for plasma [^{3}H]glucose measurement. The liver, skeletal muscle, and adipose tissue were harvested at the end of the clamp experiment to assess insulin signaling, as we have previously described (23).

Measurement of the VLDL-triglyceride secretion rate. Very low-density lipoprotein (VLDL) secretion rates *in vivo* were measured as we previously described (4). Briefly, 16-h-fasted mice were injected with Triton WR1339 (500 mg/kg in saline), a lipoprotein lipase inhibitor that inhibits VLDL hydrolysis, via the tail vein. Plasma samples were collected at 0 and 90 min after injection, and the triglyceride levels were measured. The VLDL secretion rate was calculated by subtracting triglyceride levels at 0 min from their corresponding levels at 90 min.

Liver tissue lipid analysis. Liver tissue lipid analysis was performed using the chloroform-methanol extraction method of Folch et al. (24). The lipid pellets were dissolved in a mixture of 60 μl of tert-butyl alcohol and 40 μl of Triton X-114/methanol (2:1). Triglyceride and cholesterol levels were measured using assay kits from Stanbio (Boerne, TX).

Hepatic prostaglandins and AA metabolite analysis. Hepatic prostaglandins (PGs), including PEGF2α, PGE2, PGD2, 6-kPGF1, and 20-hydroxyeicosatetraenoic acid (20-HETE), and their precursor arachidonic acids (AAs) were measured by using an MSQ single-quadrupole mass spectrometer from Thermo-Finnigan (San Jose, CA), as we have previously described (25, 26).

Body composition. The animals' body composition, including fat mass, lean mass, and water mass, was measured by EchoMRI (Houston, TX).

Primary-hepatocyte preparation and *in vitro* glycogen synthesis assay. Primary mouse hepatocytes were isolated by collagenase perfusion, as we have previously described (4). For the glycogen synthesis assay, primary hepatocytes were washed with phosphate-buffered saline (PBS) three times and then incubated with Dulbecco's modified Eagle's medium (DMEM) without glucose and pyruvate for 2 h to deplete glycogen. After 2 h, the control cells (for the measurement of basal glycogen) were washed with PBS three times and frozen at −20°C until further analysis. The remaining cells were incubated with DMEM plus 25 mM glucose and 100 nM insulin for 2 h. The cells were washed with PBS three times, and 400 μl of 2 M HCl was added per well; then, the cells were scraped and incubated at 95°C to hydrolyze the glycogen into free glucose. Duplicates of the cells were treated with 400 μl of 2 M NaOH, scraped, and incubated at 95°C for 1 h for free-glucose control. After the incubation, the HCl was neutralized with an equal volume of 2 M NaOH, and the NaOH samples were neutralized with an equal volume of 2 M HCl. Glucose concentrations were measured with a glucose kit from Sigma, and the results were normalized by protein concentrations (27).

Liver tissue glycogen content analysis. Ten milligrams of frozen liver tissues from control and fasted mice fed with a chow diet or HFD was pulverized in liquid nitrogen and then used in subsequent extraction and quantification of liver glycogen levels, as previously described (28). The liver glycogen levels were also evaluated by periodic acid-Schiff (PAS) glycogen staining.

Northern blot, real-time PCR, and Western blot analyses. Total RNA was isolated using TRIzol reagent (Invitrogen, Carlsbad, CA). Northern hybridization using a ^{32}P-labeled cDNA probe was performed as we previously described (21). SYBR green-based real-time PCR was performed with the ABI 7300 real-time PCR system. The data were normalized against cyclophilin. For Western blot analysis, 3 μl (100 μg of protein) of plasma or 30 μg of protein extracts was separated on SDS-PAGE gels and transferred onto a nitrocellulose or polyvinylidene difluoride (PVDF) membrane. The primary antibodies used were anti-ApoB100 (H-15) and anti-ApoB48 (S-18) from Santa Cruz (Dallas, TX); anti-CD36 (NB400-144) from Novus (Littleton, CO); anti-PP1Cγ (ab134947) from Abcam (Cambridge, MA); anti-AMPKα, phospho-AMPKα (Thr172), anti-gly-

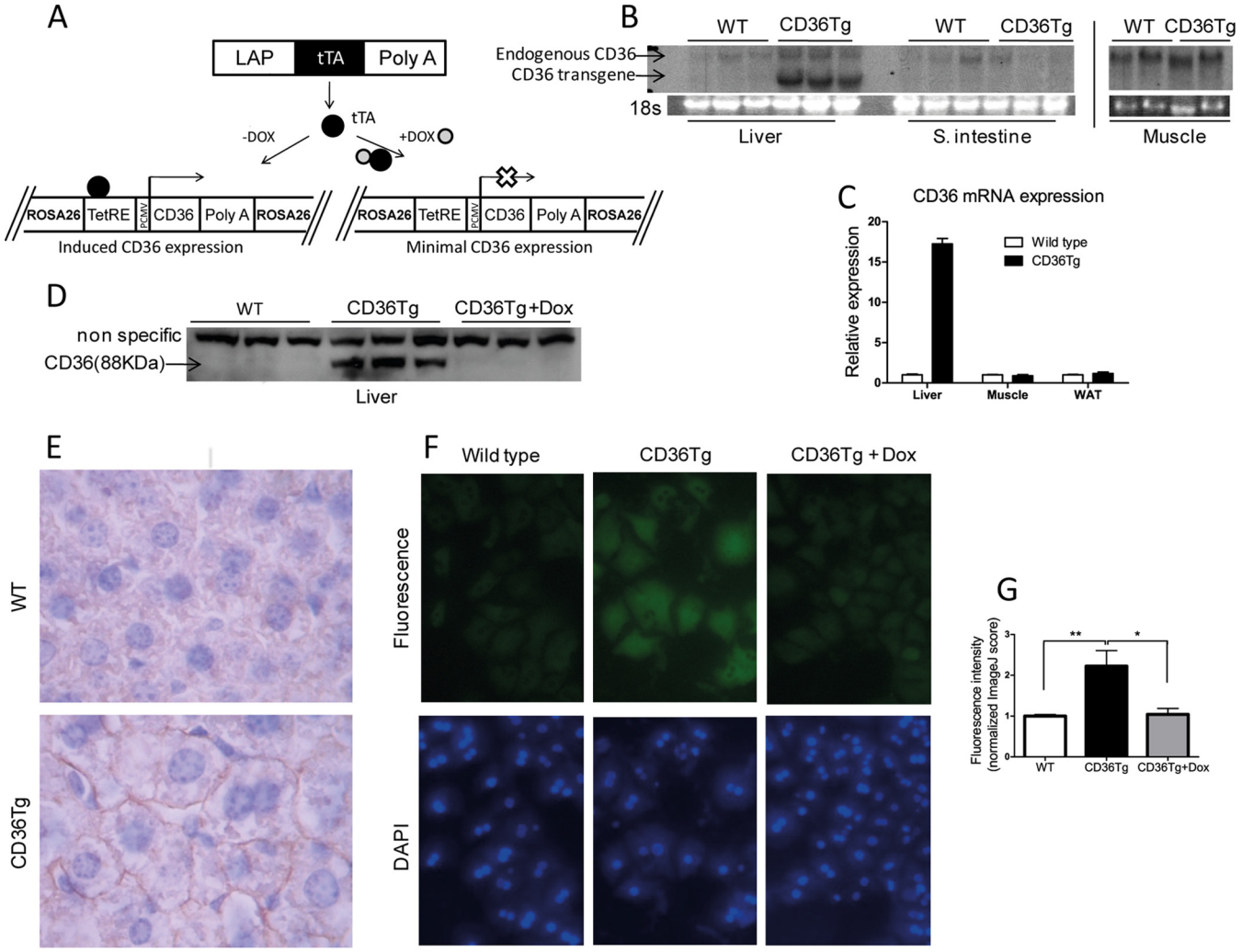

FIG 1 Creation of CD36Tg mice that overexpress CD36 in the liver. (A) Tet-off transgenic system to express CD36 in the liver. The open X indicates the silence of transgenic CD36 expression. (B and C) The mRNA expression of endogenous and transgenic CD36 (B) and transgenic CD36 (C) was detected by Northern blotting and real-time PCR, respectively. The Northern blotting probe detected both endogenous and transgenic CD36, whereas the real-time PCR specifically detected transgenic CD36. (D) Protein expression of the transgene and its silencing by Dox were measured by Western blotting. (E) Immunohistochemical staining of CD36. (F) Uptake of the fluorescent fatty acid analogue BODIPY-C16 by hepatocytes isolated from WT mice and CD36Tg mice treated or not treated with Dox. (G) Fluorometric quantification of BODIPY-C16 uptake. All the mice were maintained on a chow diet. *, $P < 0.05$; **, $P < 0.01$. The data are presented as means and SEM.

cogen synthase (3886), anti-phospho-glycogen synthase Ser641 (3891), and anti-α-tubulin (2144) from Cell Signaling (Boston, MA); anti-GSK3β (sc-9166), anti-phospho-GSK-3β (ser9) (sc-11757), and anti-glycogen phosphorylase (sc-46347) from Santa Cruz; and anti-β-actin (A1978) from Sigma.

Histology and Oil Red O staining. The general histology was evaluated by hematoxylin and eosin (H&E) staining. For Oil Red O staining, liver tissues were embedded in optimal-cutting-temperature compound, sectioned into 8-μm-thick cryosections, and stained with Oil Red O (0.5% in isopropanol) from Sigma-Aldrich.

Statistics. Statistical analysis was performed using the unpaired Student *t* test in GraphPad Prism software (San Diego, CA). The statistical significance threshold was set at a *P* value of <0.05. The data are presented as means and standard errors of the means (SEM).

Study approval. The Central Animal Facility of the University of Pittsburgh is fully accredited by the AALAC. All procedures were performed in accordance with relevant federal guidelines and with the approval of the University of Pittsburgh ethical committee.

RESULTS

Creation of CD36Tg mice that overexpress CD36 in the liver. To study the hepatic function of CD36 *in vivo*, we generated inducible and liver-specific CD36Tg mice using the Tet-Off system, as outlined in Fig. 1A. A single copy of the TetRE-CD36 transgene was site-specifically knocked into the mouse *ROSA26* gene locus via homologous recombination. The resulting TetRE-CD36 transgenic mice were then bred with liver-specific LAP-tTA transgenic mice expressing tTA under the control of the LAP (C/EBPβ) gene promoter (21). The liver/hepatocyte-specific expression of the *CD36* transgene was confirmed by Northern blotting (Fig. 1B) and real-time PCR analysis (Fig. 1C). Transgene expression was undetectable in extrahepatic tissues, such as the small intestine, skeletal muscle, and white adipose tissue (WAT) (Fig. 1B and C). The protein expression from the transgene was verified by Western blotting, and as expected, treatment of the CD36Tg mice with Dox

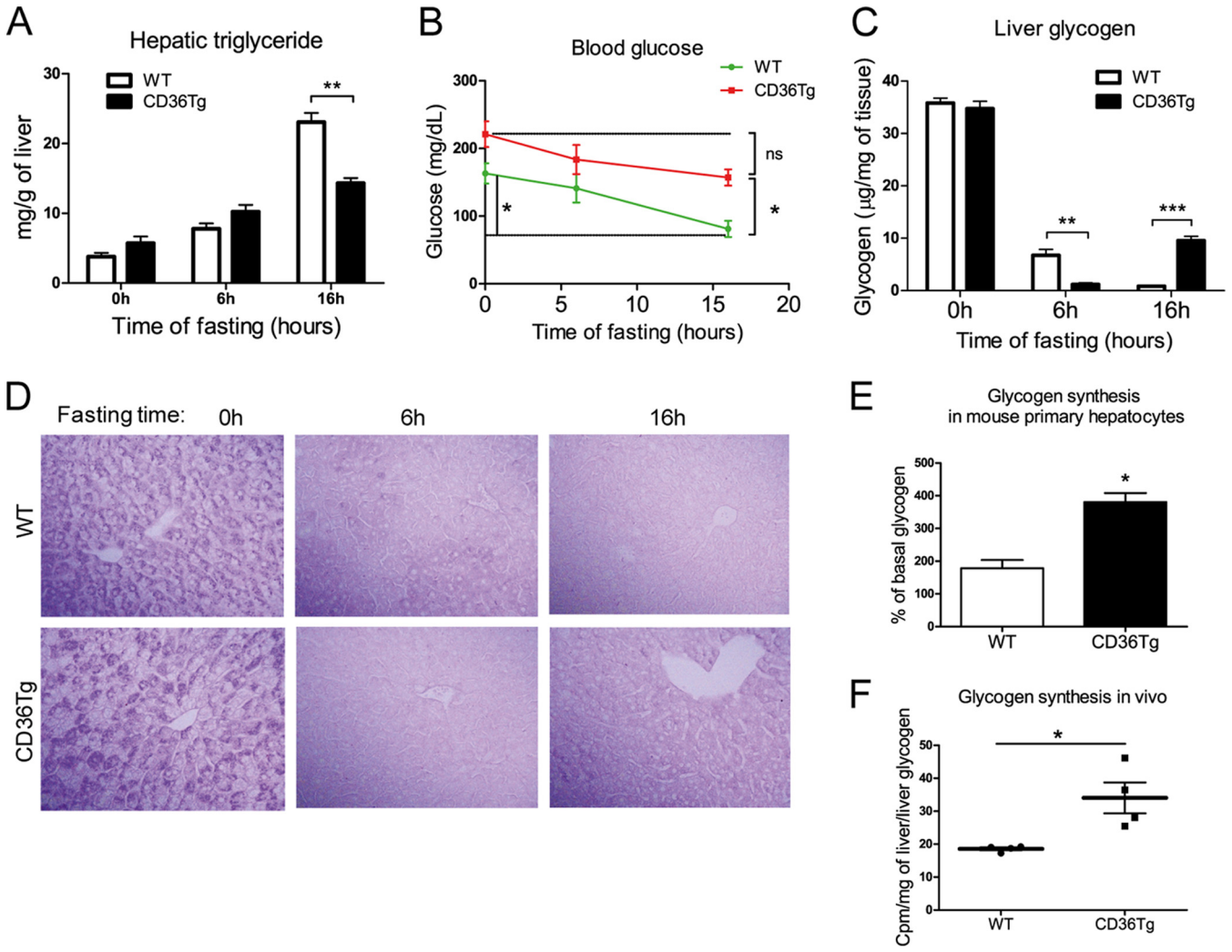

FIG 2 Overexpression of CD36 attenuated the fasting-induced steatosis, hypoglycemia, and depletion of hepatic glycogen. (A to D) Mice maintained on a chow diet were subjected to 6 h and 16 h of fasting before measurement of liver triglyceride levels (A), blood glucose (B), liver glycogen levels (C), and liver PAS staining (D). $n = 4$ for all groups. (E) Insulin- and glucose-stimulated glycogen synthesis rates in primary mouse hepatocytes. (F) Incorporation of [^{3}H]glucose into hepatic glycogen during the euglycemic-hyperinsulinemic clamp. WT, $n = 7$; CD36Tg, $n = 6$. *, $P < 0.05$; **, $P < 0.01$; ***, $P < 0.001$; ns, statistically not significant. The data are presented as means and SEM.

silenced transgene expression (Fig. 1D). CD36 transgenic protein expression was estimated to be 16 times the endogenous CD36 level when mice were maintained on a chow diet (Fig. 1D). Immunohistochemistry showed that the overexpressed CD36 had a predominant hepatocyte membrane distribution (Fig. 1E), which rendered the CD36 protein a functional translocase (7). The functionality of the transgenic CD36 protein was confirmed in primary hepatocytes, where the uptake of BODIPY-C16, a fluorescent fatty acid analogue and substrate of CD36 (4), was higher in CD36Tg hepatocytes than in the WT or CD36Tg hepatocytes treated with Dox (Fig. 1F and G).

Overexpression of CD36 attenuated fasting-induced steatosis, hypoglycemia, and depletion of hepatic glycogen. Surprisingly, the CD36Tg mice maintained on a chow diet did not show obvious signs of fatty liver. We then subjected the mice to the metabolic stress of fasting, which is known to induce acute hepatic steatosis (29), and compared the steatotic phenotype to that of the WT mice. Under the basal conditions and after 6 h of fasting, the CD36Tg mice had marginally higher levels of liver triglycerides than their WT counterparts (Fig. 2A). However, after 16 h of fasting, the CD36Tg mice had significantly lower hepatic triglyceride levels (Fig. 2A), which was not associated with increased VLDL secretion (data not shown). Fasting is also known to induce hypoglycemia and depletion of hepatic glycogen (30). As expected, WT mice showed significantly decreased blood glucose levels after the 16-h fast (Fig. 2B). In contrast, the fasting-responsive fall in blood glucose in the CD36Tg mice was not significant, and the levels were significantly higher than those of their WT counterparts (Fig. 2B). The fed glucose levels in CD36Tg mice appeared to be higher than in WT animals, but the difference was not statistically significant (Fig. 2B).

The fasting response is dependent on glycogen dynamics, and a hallmark of the fasting response is glycogen depletion (31). The basal levels of hepatic glycogen were not different between the chow-fed WT and CD36Tg mice (Fig. 2C). After fasting for 6 h, glycogen was almost completely depleted in the livers of CD36Tg

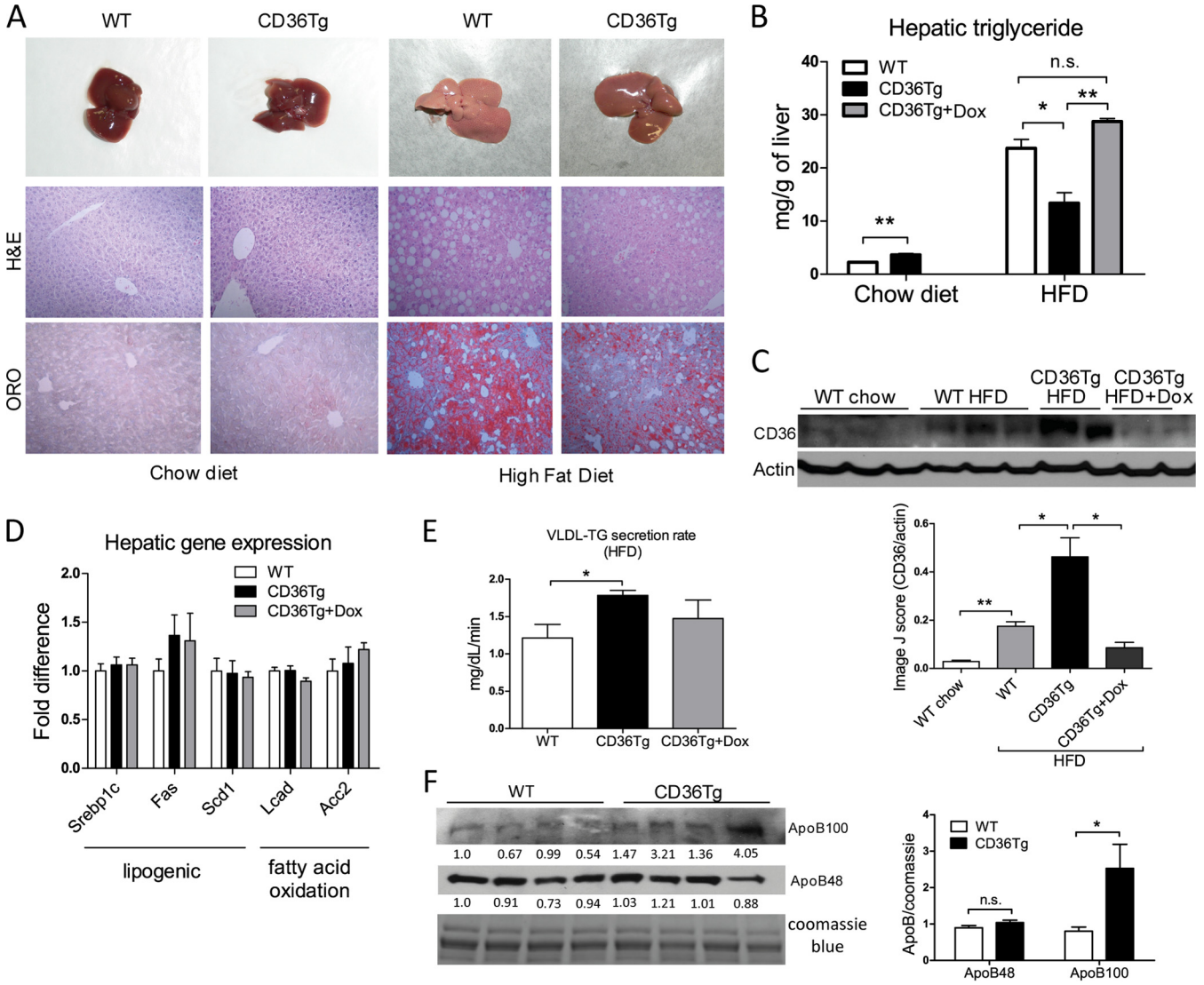

FIG 3 CD36Tg mice were protected from HFD-induced hepatic steatosis. (A) Gross appearance (top) and histology (bottom) (H&E and Oil Red O [ORO] staining) of livers of mice maintained on a chow diet (left) and mice that had been fed an HFD for 19 weeks (right). (B) Hepatic triglyceride levels in mice maintained on a chow diet and mice that had been fed an HFD for 19 weeks in the absence or presence of Dox. $n = 5$. (C) Expression of liver CD36 as measured by Western blotting. Densitometric quantifications of the blots are shown below. (D) The hepatic expression of genes involved in lipogenesis and fatty acid oxidation in HFD-fed mice was measured by real-time PCR. $n = 5$. (E) VLDL-triglyceride (TG) secretion rate in HFD-fed WT, CD36Tg, and CD36Tg-plus-Dox mice. $n = 4$. (F) The serum levels of ApoB100 and ApoB48 were measured by Western blotting. The serum samples were run on two parallel gels; one was used for Coomassie blue staining as a loading control, and the second gel was used for ApoB100/48 Western blotting. The densitometric intensity was normalized to the Coomassie blue staining. The densitometric scores for individual lanes are shown. On the right is shown statistical analysis of the densitometric quantification. *, $P < 0.05$; **, $P < 0.01$; n.s., not statistically significant. The data are presented as means and SEM.

mice, whereas in the WT mice, glycogen levels were reduced by approximately 80%, but a substantial amount still remained. After fasting for 16 h, glycogen was essentially exhausted in the WT mice, while in contrast, it had been restored to approximately 35% of the prefasting levels in the CD36Tg mice (Fig. 2C). The dynamics of fasting glycogen levels were confirmed by periodic acid-Schiff staining (Fig. 2D). These results suggested that overexpression of CD36 in hepatocytes promoted glycogen synthesis during prolonged starvation and led to partial recovery of this important energy store.

To determine whether overexpression of CD36 was sufficient to induce glycogen synthesis, we went on to directly measure glycogen synthesis in isolated primary hepatocytes *in vitro*. Insulin is known to promote hepatic glucose uptake and glycogen synthesis (32). In response to high glucose and insulin stimulation, glycogen synthesis in primary hepatocytes from CD36Tg mice was twice that in hepatocytes from WT mice (Fig. 2E). Although this *in vitro* glycogen synthesis model does not mimic the fasting condition, our results suggested that CD36 overexpression was sufficient to affect glycogen synthesis. CD36Tg mice also showed increased glycogen synthesis *in vivo*, because under the euglycemic-hyperinsulinemic clamp condition, the hepatic synthesis of glycogen was higher in CD36Tg mice than in WT mice (Fig. 2F).

TABLE 1 Serum biochemistry of WT, CD36Tg, and CD36Tg-plus-Dox mice fed chow diet or HFD for 19 weeks

Parameter	Value for:					
	Chow diet-fed mice			HFD-fed mice		
	WT ($n = 5$)	CD36Tg ($n = 4$)	CD36Tg + Dox ($n = 4$)	WT ($n = 7$)	CD36Tg ($n = 6$)	CD36Tg + Dox ($n = 4$)
Total cholesterol (mg/dl)	114.3 ± 16.2	114.6 ± 8.8	119.2 ± 9.3	129.4 ± 22.1	165 ± 15.6[b]	137.9 ± 14.5
Triglyceride (mg/dl)	51.8 ± 10.2	49.9 ± 9.5	58.5 ± 4.4	75.2 ± 20.0[c]	75.0 ± 7.7	75.2 ± 7.7
Free fatty acids (μM)	318.5 ± 86.9	294 ± 101.8	347.2 ± 151	496 ± 94.7[d]	526.5 ± 158.9	698.1 ± 145.9
ALT (U/liter)	26.4 ± 5.0	30.7 ± 7.3	21.4 ± 12.8	65.2 ± 6.7[d]	45.7 ± 17.4[a]	82.5 ± 30.0
AST (U/liter)	62.9 ± 20.1	68.9 ± 10.7	71.0 ± 14.3	225.7 ± 38.8[d]	166.4 ± 17.6[a]	265.9 ± 65.1
Fasting blood glucose (mg/dl)	128.7 ± 17.2	143.8 ± 3.2	127.4 ± 14.2	187.9 ± 35.6[c]	190.1 ± 24.2	183.9 ± 23.3
Fasting insulin (ng/ml)	0.4 ± 0.1	0.6 ± 0.5	0.4 ± 0.08	8.3 ± 4.08[d]	12.4 ± 6.1	6.1 ± 2.0

[a] $P < 0.05$ compared to the WT within the diet group.
[b] $P < 0.01$ compared to the WT within the diet group.
[c] $P < 0.05$ for WT mice fed an HFD compared to WT mice fed chow to validate the HFD model.
[d] $P < 0.01$ for WT mice fed an HFD compared to WT mice fed chow to validate the HFD model.

CD36Tg mice were protected from HFD-induced hepatic steatosis. We then challenged mice with an HFD, another metabolic stress, and a model of fatty liver, obesity, and type 2 diabetes. When mice were maintained on a chow diet, there were no obvious differences in the gross appearance and histology of the liver between the WT and CD36Tg mice (Fig. 3A, left). Upon 19-week HFD feeding, the CD36Tg liver appeared less fatty, which was confirmed by H&E and Oil-Red O staining (Fig. 3A, right). Indeed, CD36Tg mice had a modest but significant increase in liver triglyceride levels when maintained on a chow diet. Upon HFD feeding, the liver triglyceride levels in CD36Tg mice were significantly lower than in their WT counterparts, and this effect was abolished by Dox treatment (Fig. 3B). When the expression of CD36 was examined, we found the expression of hepatic CD36 in WT mice was induced by HFD feeding (Fig. 3C), consistent with a previous report (3). The hepatic expression of CD36 in the HFD-fed CD36Tg mice was approximately 2.5 times that in the HFD-fed WT mice (Fig. 3C). These results suggested that the elevated expression of hepatic CD36 is not a sufficient explanation for the HFD-responsive steatosis. It was noted that the HFD effect on the expression of endogenous CD36 was somehow diminished in Dox-treated CD36Tg mice, perhaps through yet to be defined feedback regulation of endogenous CD36.

In investigating the molecular basis for the attenuated HFD-induced steatosis in CD36Tg mice, we found the expression of major genes involved in *de novo* lipogenesis and fatty acid β-oxidation was not different in the HFD-fed CD36Tg and WT mice (Fig. 3D). Instead, the VLDL-triglyceride secretion rate in the HFD-fed CD36Tg mice was significantly higher than in the WT mice, and this effect was attenuated by Dox treatment (Fig. 3E). The level of lipoprotein ApoB100 (liver origin), an essential component of the VLDL particles, in serum was increased, whereas the level of ApoB48 (intestine origin) in serum was not affected (Fig. 3F). These results suggested that increased liver triglyceride export might have contributed to the overall attenuation of the HFD-induced steatosis in the CD36Tg mice. The increase of VLDL secretion in the CD36Tg mice was also consistent with the reduction of VLDL secretion recently reported for $CD36^{-/-}$ mice (10).

Analysis of serum biochemistry revealed transgene-dependently decreased levels of alanine aminotransferase (ALT) and aspartate aminotransferase (AST) in HFD-fed CD36Tg mice (Table 1), consistent with the relief of hepatic steatosis in the genotype. The triglyceride level was not affected by the transgene despite the increased VLDL secretion, suggesting increased clearance of triglycerides from the circulation. CD36Tg mice also showed a transgene-dependent increase in total serum cholesterol, the mechanism of which remains to be understood. The fasting blood glucose, serum free fatty acid, and fasting insulin levels were not significantly affected by the transgene in the HFD groups (Table 1).

Overexpression of CD36 attenuated HFD-induced insulin resistance. When mice were treated with an HFD, the CD36 transgene had little effect on body weight gain (Fig. 4A), fat mass gain (Fig. 4B), or food intake (Fig. 4C). Metabolic cage analysis showed that the CD36Tg mice had increased oxygen consumption during the dark phase (Fig. 4D). However, the respiratory exchange ratio (RER) (Fig. 4E) and locomotive movement (Fig. 4F) were not affected. The heat generated (Fig. 4G) showed a trend toward increase, but the difference did not reach statistical significance. In addition, the HFD-fed CD36Tg mice showed significantly improved performance in the GTT (Fig. 4H) and ITT compared with WT mice (Fig. 4I), and both benefits were abolished upon Dox treatment.

To assess the effects of CD36 on hepatic and peripheral insulin sensitivity, we performed the hyperinsulinemic euglycemic clamp experiment on HFD-fed mice. Compared to the WT mice, the CD36Tg mice required approximately double the amount of glucose infusion to maintain euglycemia (Fig. 5A), indicating enhanced insulin-stimulated glucose uptake and metabolism in the genotype. When glucose production was measured, the CD36Tg mice exhibited dramatic suppression of hepatic glucose production under the insulin-stimulated clamp state (Fig. 5B), suggesting an enhancement of hepatic insulin sensitivity. Additionally, the glucose disposal rate under the clamp state was significantly higher in the CD36Tg mice (Fig. 5C). To directly assess the insulin effect, we injected mice i.p. with insulin, and the livers were collected for the measurement of Akt phosphorylation by Western blotting. As shown in Fig. 5D, the CD36Tg mice showed increased basal and insulin-responsive Akt phosphorylation in the liver. Consistent with their increased glucose tolerance (Fig. 4H) and insulin sensitivity (Fig. 4I and 5A to C) and decreased glucose production during the hyperinsulinemic euglycemic clamp (Fig. 5B), the CD36Tg mice showed an overall suppression of hepatic genes that are involved in gluconeogenesis, including significant inhibition of peroxisome proliferator-activated receptor γ coacti-

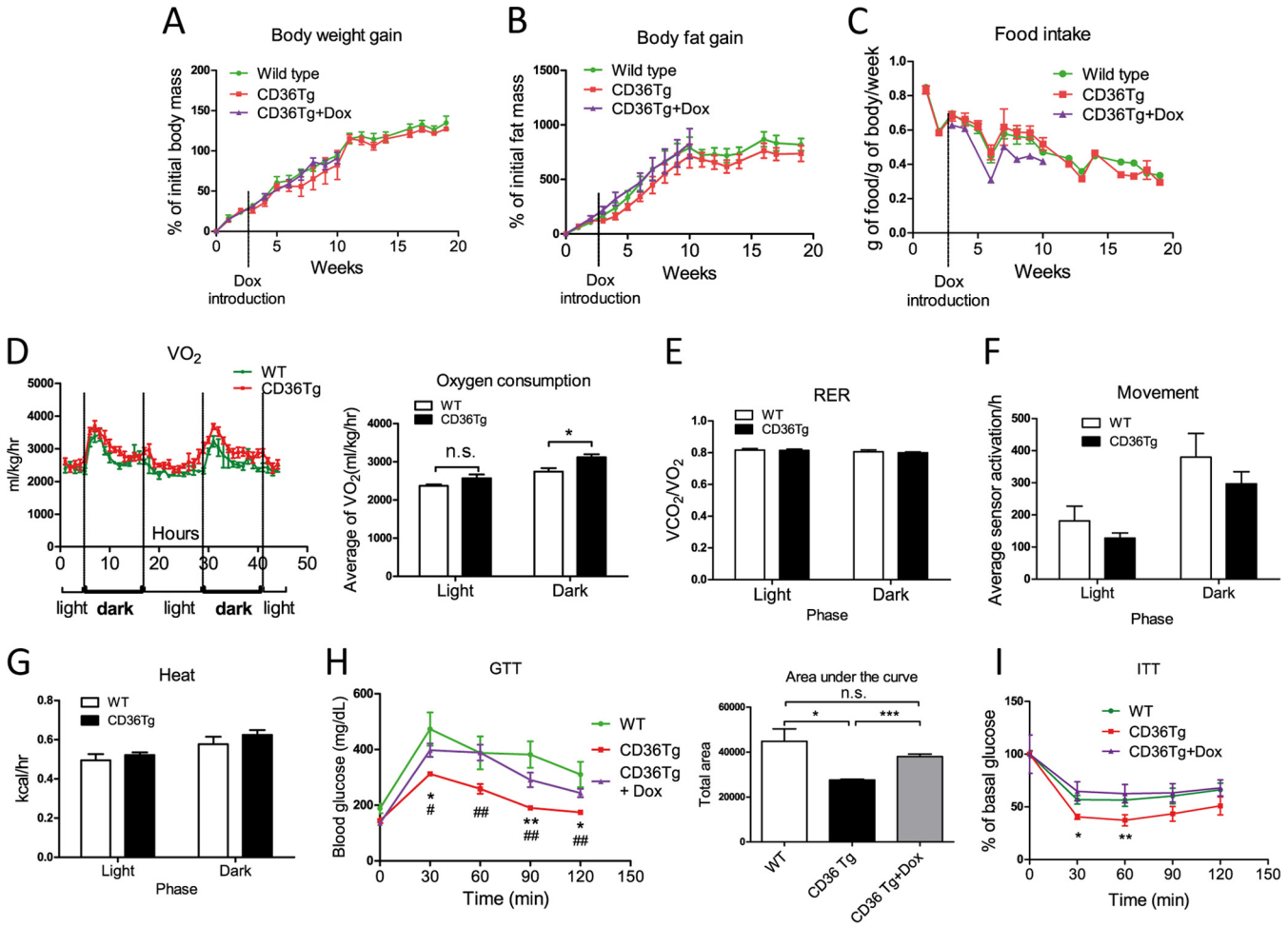

FIG 4 CD36 overexpression improved glucose homeostasis and increased oxygen consumption. All the mice were fed an HFD for 19 weeks. (A to C) HFD-responsive dynamics of body weight gain (A), fat mass gain as measured by magnetic resonance imaging (MRI) (B), and food intake (C) in WT mice and CD36Tg mice treated or not treated with Dox. $n = 7$ to 9. (D) Oxygen consumption throughout the light-dark cycle. $n = 4$. (E to G) Metabolic cage analysis of RER (E), locomotive movement (F), and heat generated (G). $n = 4$. (H and I) GTT (H) and ITT (I) in WT mice and CD36Tg mice treated or not with Dox. The area under the curve (AUC) was used to quantify the GTT results. $n = 5$. * and #, $P < 0.05$; ** and ##, $P < 0.01$; n.s., not statistically significant. The asterisks and hash tags are comparisons between WT and CD36Tg and between CD36Tg and CD36Tg-plus-Dox mice, respectively. The data are presented as means and SEM.

vator 1α (PGC1α) and glucose 6-phosphatase (G6Pase) gene expression, which was abolished upon Dox treatment (Fig. 5E).

Interestingly, the metabolic benefit of the transgene was also observed in skeletal muscle, despite the lack of transgene targeting in the tissue. Basal Akt phosphorylation in skeletal muscle was markedly increased in CD36Tg mice, but acute treatment with insulin did not lead to a further increase (Fig. 5D). The skeletal muscle tissues harvested under the clamp (i.e., under continuous insulin infusion) also showed a higher level of Akt phosphorylation in the CD36Tg mice (data not shown). The metabolic benefits of the transgene in skeletal muscle were also supported by the decreased tissue triglyceride levels (Fig. 5F), decreased expression of the lipogenic Srebp-1c gene, increased expression of fatty acid oxidative long-chain fatty acid acyl coenzyme A (acyl-CoA) dehydrogenase (Lcad) (Fig. 5G), and decreased expression of genes indicative of inflammation, such as the tumor necrosis factor alpha (TNF-α) gene (data not shown). Expression in muscle of carnitine palmitoyltransferase I (Cpt1) and PPARα also tended to be higher (Fig. 5G). Meanwhile, the muscle mRNA expression of lipoprotein lipase (LPL), which hydrolyzes triglycerides, was significantly increased in CD36Tg mice, whereas expression of the glucose uptake transporter GLUT4 was not affected (Fig. 5H). In skeletal muscle, the glycogen contents were not different between the WT and CD36Tg mice (Fig. 5I), suggesting that the glycogen phenotype was liver specific.

The induction of LPL appeared to be skeletal muscle specific, because the expression of LPL in WAT was not affected by the transgene (Fig. 5J). The expression in adipose tissue of hormone-sensitive lipase (HSL), adipose triglyceride lipase (ATGL), angiopoietin-like 4 (ANGPTL4), perilipin, and adiponectin tended to be higher in CD36Tg mice, but the differences did not reach statistical significance (Fig. 5J). The morphology of adipocytes in WAT was not affected (data not shown).

Molecular mechanism for the promotion of glycogen synthesis by CD36. To understand how glycogen synthesis was enhanced in the CD36Tg mice, we first examined the mRNA expression of genes that are involved in glycogen synthesis and breakdown during fasting. Glycogenin initiates the synthesis of glycogen poly-

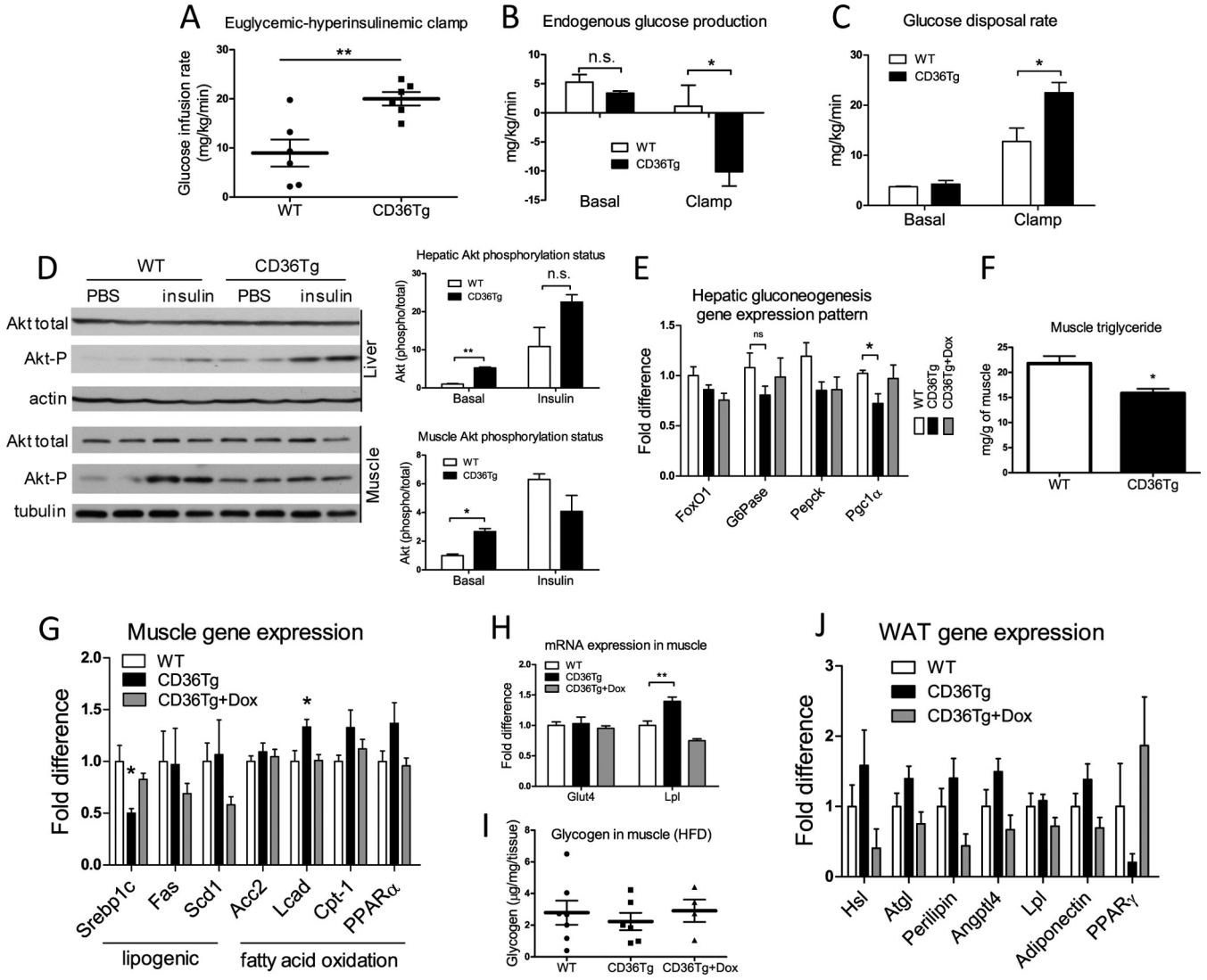

FIG 5 Hepatic overexpression of CD36 attenuated HFD-induced insulin resistance. The mice are the same as those described in the legend to Fig. 4. (A to C) Euglycemic-hyperinsulinemic clamp measurements of glucose infusion rate (A) endogenous glucose production (B), and glucose disposal rate (C) in HFD-fed WT mice and CD36Tg mice. $n = 6$ or 7. (D) Basal and insulin-stimulated Akt phosphorylation in liver and skeletal muscle as measured by Western blotting. Shown on the right are densitometric quantifications of the blots. When necessary, mice were injected i.p. with insulin (0.75 U/kg) 17 min before tissue harvesting. (E) Hepatic mRNA expression of gluconeogenic genes. $n = 6$. (F to I) Triglyceride level (F), expression of genes involved in lipogenesis and fatty acid oxidation (G), expression of the glucose transporter GLUT4 and LPL (H), and glycogen content (I) in skeletal muscle. $n = 6$. (J) WAT mRNA expression of genes indicative of adipocyte remodeling and metabolism. $n = 6$. *, $P < 0.05$; **, $P < 0.01$; n.s., statistically not significant. The data are presented as means and SEM.

mers from glucose molecules, whereas GS is the rate-limiting enzyme for glycogen synthesis. As expected, the expression of both genes tended to increase during fasting, but the relative levels of expression were not statistically different in WT, CD36Tg, and CD36Tg-plus-Dox mice (Fig. 6A). GP is responsible for the breakdown of glycogen and the release of glucose. The expression of GP was largely unaffected by either fasting or the genotype (Fig. 6A). These results suggested that the promoting effect of CD36 on glycogen dynamics might not occur at the transcriptional level. When the protein expression of GP was measured, we found that hepatic GP levels were significantly higher in the CD36Tg mice after 6 h of fasting (Fig. 6B), likely through a yet to be defined posttranscriptional mechanism. The levels of GP in Dox-treated CD36Tg mice were similar to those in the WT mice. Since the activity of GP is also regulated by phosphorylation, we cannot simply conclude that the increased GP protein expression had contributed to the accelerated glycogen breakdown or resistance to fasting-induced hypoglycemia in CD36Tg mice.

The activity of GS is known to be regulated by phosphorylation (33) and partly by allosteric interactions with glucose-6-phosphate (G6P) (14). The phosphorylation of GS was dramatically different between WT and CD36Tg mice. In WT mice, the expression of GS protein increased steadily with the fasting time, and this was mirrored by the decrease in Ser641 phosphorylation of GS, rendering the enzyme more active (Fig. 6B). However, in the livers of CD36Tg mice, the GS protein was not only more abundant but also constitutively dephosphorylated (and thus activated) regardless of fasting time (Fig. 6B). The decreased phosphorylation of GS

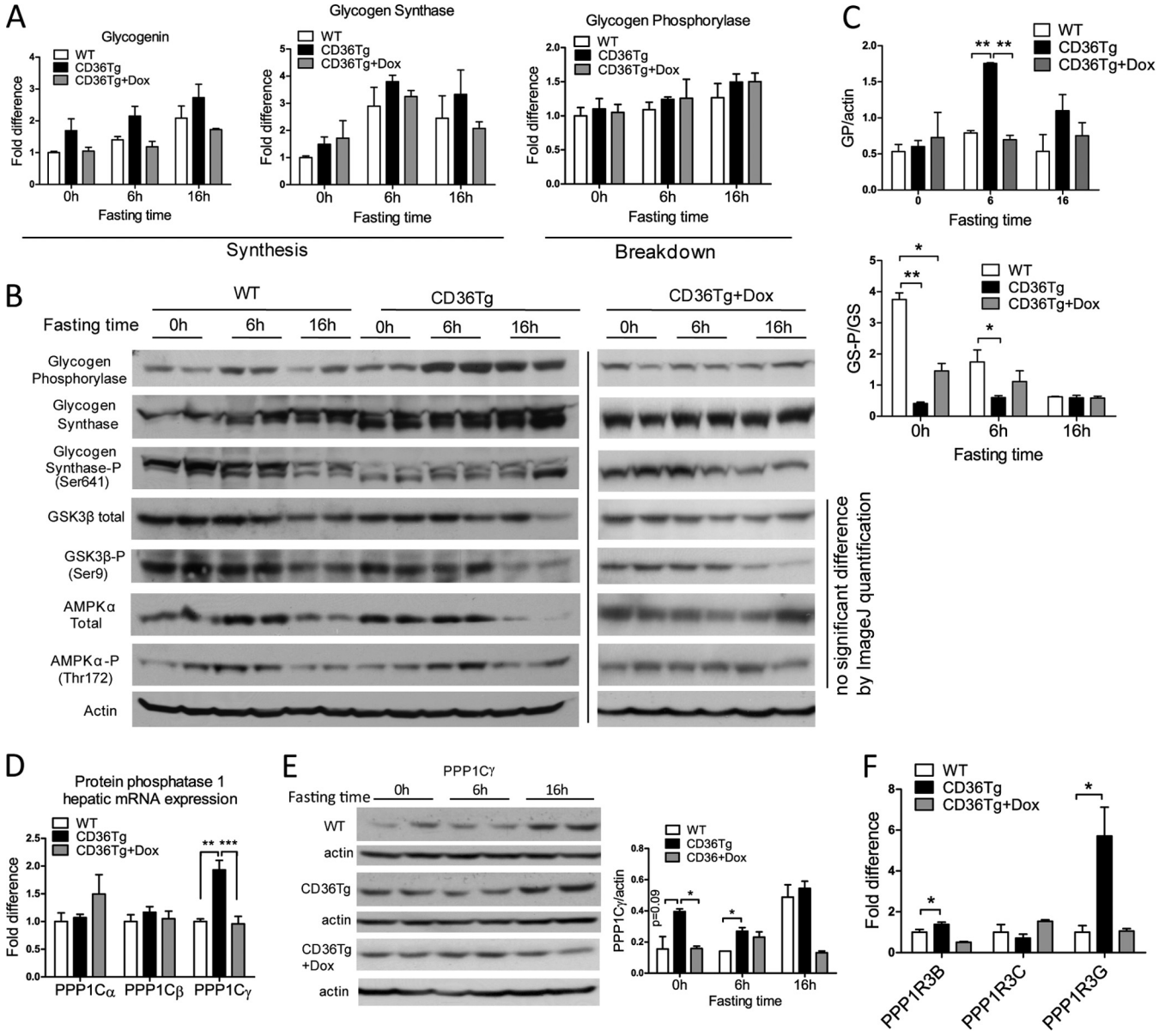

FIG 6 Molecular mechanism for promoting glycogen synthesis by CD36. WT, CD36Tg, and CD36Tg-plus-Dox mice maintained on a chow diet were subjected to 6 h and 16 h of fasting. (A) The hepatic mRNA expression of glycogenin, GS, and glycogen phosphorylase genes was measured by real-time PCR. (B) The protein expression of GP, total and Ser641-phosphorylated GS, total and Ser9-phosphorylated GSK3β, and total and phosphorylated AMPKα was measured by Western blotting. (C) Densitometric quantification of GP and GS-P/GS expression. (D) mRNA expression of PP1 catalytic subunits (PPP1Cs). (E) Protein expression of PPP1Cγ as measured by Western blotting. Shown on the right are densitometric quantifications of the blots. (F) mRNA expression of PPP1R3B, PPP1R3C, and PPP1R3G regulatory glycogen targeting subunits of PP1. $n = 4$ for all groups. *, $P < 0.05$; **, $P < 0.01$; ***, $P < 0.001$; n.s., statistically not significant. The data are presented as means and SEM.

in CD36Tg mice was attenuated upon Dox treatment (Fig. 6B). The densitometric quantifications of the protein expression of GP and phosphorylated GS (GS-P)/GS are shown in Fig. 6C. The phosphorylation of GS is primarily mediated by GSK3β at Ser641, but it can also be mediated by AMPK and protein kinase A (PKA). The activities of these kinases are also regulated by phosphorylation (34). We found that the total protein and phosphorylation of GSK3β and AMPKα were not significantly affected by the CD36 genotype (Fig. 6B).

The lack of evidence that upstream kinase is responsible for the altered GS phosphorylation during fasting prompted us to examine the effect of the *CD36* transgene on the expression of PP1. PP1 is responsible for the dephosphorylation and activation of GS (35, 36). PP1 consists of three catalytic subunits, Cα, Cβ, and Cγ. We found that the basal mRNA expression of phosphoprotein phophatase 1 catalytic subunit gamma (PPP1Cγ) was significantly upregulated in the liver in CD36Tg mice, but the expression of two other catalytic subunits was not significantly affected (Fig. 6D). The higher expression of PPP1Cγ protein in the CD36Tg mice was confirmed by Western blotting (Fig. 6E). The substrate specificity of PP1 is achieved by its association with regulatory subunits, such as PPP1R3B, PPP1R3C, and PPP1R3G (15,

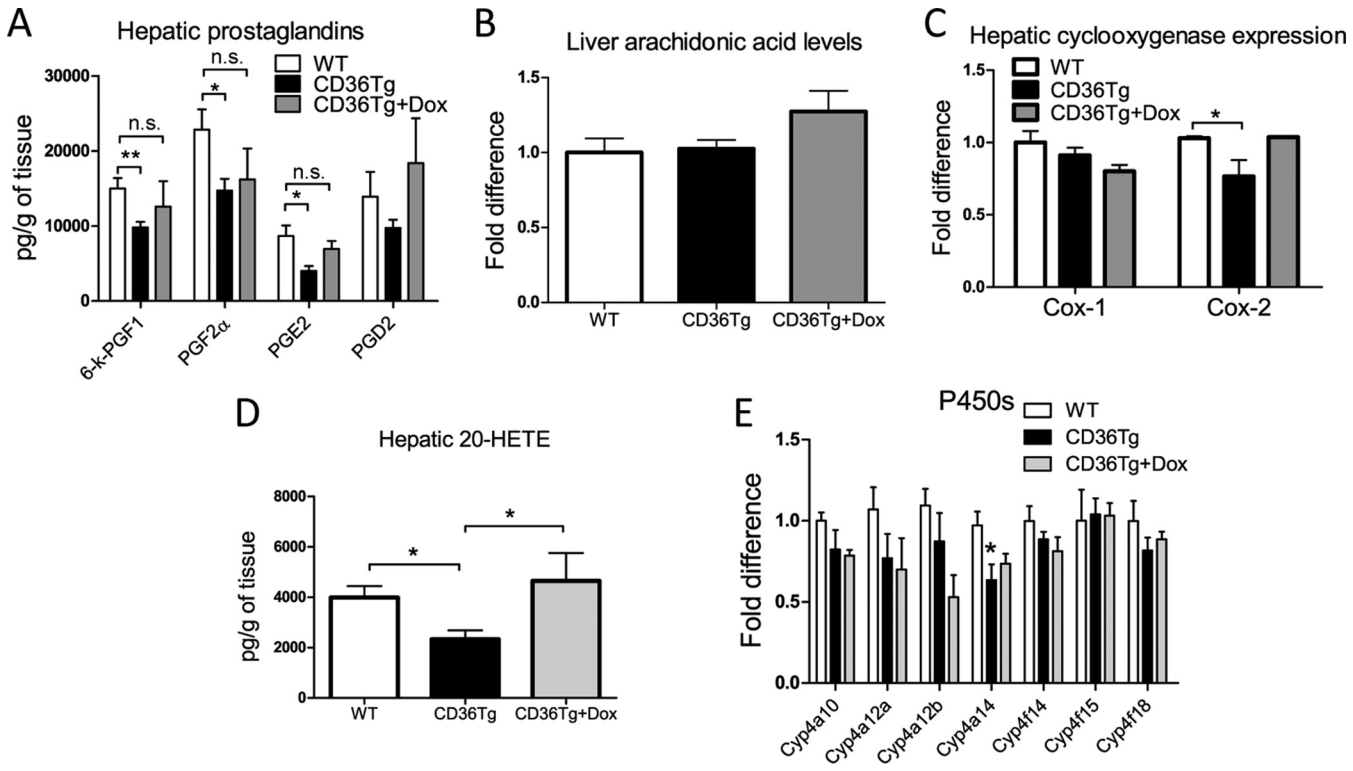

FIG 7 Overexpression of CD36 affected arachidonic acid metabolism and decreased hepatic levels of prostaglandins and 20-HETE. All the mice were fed an HFD for 19 weeks, and the CD36Tg mice were treated or not treated with Dox. (A) Hepatic prostaglandin levels. (B) Hepatic arachidonic acid levels. (C) Hepatic expression of Cox-1 and Cox-2. (D) Hepatic 20-HETE level. (E) Hepatic expression of 20-HETE-producing Cyp4a/Cyp4f enzymes. $n = 6$ for all groups. *, $P < 0.05$; **, $P < 0.01$; n.s., not statistically significant. The data are presented as means and SEM.

35). The hepatic mRNA expression of PPP1R3B and PPP1R3G was significantly upregulated in CD36Tg mice in a transgene-dependent manner, but the expression of PPP1R3C was not affected (Fig. 6F).

Overexpression of CD36 affected arachidonic acid metabolism and decreased hepatic levels of prostaglandins and 20-HETE. PGs are catabolic metabolites of AA. CD36 signaling has been suggested to play a role in the liberation of AA and subsequent formation of PGs (37). Increased levels of hepatic PGs can negatively affect the hepatic export of VLDL (10, 38). We found that HFD-fed CD36Tg mice had significantly reduced hepatic PGE2, PGF2α, and 6-keto-PGF1 levels compared to their WT controls and the CD36Tg-plus-Dox group (Fig. 7A). The decreased PG levels were not due to the lack of AA substrate, because the levels of AA were similar in WT and CD36Tg mice (Fig. 6B), but rather was associated with decreased expression of cyclooxygenase 2 (Cox-2) in the liver (Fig. 7C). In addition to the formation of PGs, terminal hydroxylation of AA yields the potent vasoconstrictive and proinflammatory eicosanoid 20-HETE (25). 20-HETE can induce hyperglycemia through the cAMP/PKA-PhK-GP pathway (39), and 20-HETE levels have been positively associated with liver cirrhosis (40). We found that the hepatic 20-HETE level was significantly reduced in CD36Tg mice, but it was restored to the WT level upon Dox treatment (Fig. 7D). The metabolism of AA to 20-HETE is catalyzed by the CYP4A/4F enzymes. We found that the expression of Cyp4a14 was significantly lower in CD36Tg mice (Fig. 7E).

DISCUSSION

Despite the well-documented function of CD36 in fatty acid uptake (41) and several reports that associate hepatic CD36 signaling with an increased risk of developing liver steatosis (3, 5, 6, 8, 42), we showed that overexpression of CD36 in the livers of our transgenic mice did not worsen metabolic functions but rather protected the mice from the detrimental metabolic changes caused by HFD feeding and prolonged fasting. The antisteatotic effect of CD36 is consistent with a report that whole-body CD36 ablation exacerbated hepatic steatosis in the *ob/ob* background (10) but is contrary to a recent study showing that liver-specific knockout of CD36 reduced the liver lipid content when mice were challenged with HFD (42). Future studies are necessary to explain the discrepancies in the fatty liver phenotypes between the whole-body and liver-specific CD36 knockout models.

Another intriguing finding is the antidiabetic effect of the CD36 transgene, which might have been accounted for by the improved liver glycogen dynamics, as evidenced by the constitutive activation of GS, improved glycemic control, and increased insulin sensitivity in our CD36Tg mice. Hepatic glycogen homeostasis under metabolic stress is known to have a profound effect on whole-body energy homeostasis (11, 43). To explain the increased glycogen synthesis, we found that the GS protein in the CD36Tg liver was not only more abundant but also constitutively dephosphorylated and thus activated. The increased expression of the catalytic (PP1Cγ) and regulatory (PPP1R3G) subunits of PP1 might have also contributed

to the increased glycogen synthesis in the CD36Tg mice. Indeed, modulation of GS (44) or overexpression of the regulatory subunits of PP1 has been shown to relieve diabetes, obesity (15, 19), and steatosis (15). The mechanism by which CD36 affects the expression of PP1Cγ and PPP1R3G remains to be defined. Nevertheless, the improved glycogen homeostasis in CD36Tg mice might explain their protection from fasting-induced hypoglycemia, because liver glycogen breakdown and synthesis are essential in controlling blood glucose (45). In addition to the improved liver glycogen dynamics, the suppression of hepatic gluconeogenesis and the metabolic benefit in skeletal muscle may have also contributed to the antidiabetic phenotype in our CD36Tg mice. Since the CD36 transgene was specifically targeted to hepatocytes, we speculate that the metabolic benefit in skeletal muscle might be secondary to the improved liver metabolism. Although there were no changes in the respiratory exchange ratio (Fig. 4E) and locomotive movement (Fig. 4F), oxygen consumption during the dark phase was clearly increased in the transgenic mice (Fig. 4D). The CD36Tg mice also showed a tendency toward increased heat generation (Fig. 4G). The overall phenotype of the CD36Tg mice might reflect a compensatory mechanism caused by an increased triglyceride shift from the liver to the peripheral tissues, such as skeletal muscle and brown adipose tissue, in which the preferred energy source is lipids. Interestingly, despite their antidiabetic phenotype, the CD36Tg mice showed little change in body mass (Fig. 4A), fat mass (Fig. 4B), or food intake (Fig. 4C), which was consistent with the notion that animal models with enhanced glycogen synthesis reveal little change in body weight (15, 19, 20, 46).

We also observed inhibition of hepatic prostaglandin formation in our CD36Tg mice, which may have contributed to the increased glycogen synthesis. Prostaglandins, such as PGE_2 and PGF_2, have been reported to have inhibitory effects on GS (47). However, it was noted that the effect of prostaglandins on glycogen synthesis has been controversial. For example, Okumura and colleagues reported that PGE_2 can actually stimulate glycogen synthesis in rat hepatocytes, and this effect might depend on the concentrations of calcium in the incubation medium (51). Interestingly, the intracellular concentrations of calcium can be regulated by CD36 (37). Additionally, PGE_2 was reported to decrease glucagon stimulation of GP activity (16), which may help to explain the fast depletion of glycogen in CD36Tg mice during the early phase of fasting and the consequent protection from fasting-responsive hypoglycemia. Meanwhile, the constitutive activation of GS in the CD36Tg mice restored the glycogen deposits more efficiently in these mice than in the WT mice. The sources of glycogen replenishment are most likely the gluconeogenic precursors or glycerol released during lipolysis (48, 49). However, we cannot exclude the possibility that mechanisms other than the inhibition of prostaglandin formation accounted for the increased glycogen synthesis in our CD36Tg mice. Due to the lack of PG phosphorylation results, we cannot exclude the possibility that changes in the rate of glycogen breakdown also contributed to the overall improvement in glycogen homeostasis. Moreover, in the absence of an unbiased metabolomics analysis, it is not our intention to claim that changes in the prostaglandin levels are the driving force for the metabolic phenotypes of our CD36Tg mice.

The suppression of PGs may have contributed to increased VLDL secretion, because PGs are known to inhibit VLDL secretion from the liver (10, 50). The suppressed PG production and increased VLDL secretion in our CD36Tg mice were both consistent with the increased PG levels and decreased VLDL secretion reported for the *ob/ob* $CD36^{-/-}$ mice (10). It was noted that the whole-body knockout of CD36 was used in the *ob/ob* $CD36^{-/-}$ study, so we cannot exclude the possibility that a loss of CD36 in extrahepatic tissues contributed to the PG phenotype. Nevertheless, it is likely that in our CD36Tg mice, amelioration of diet- or fasting-induced steatosis resulted from a synergistic effect of enhanced glycogen turnover and increased VLDL secretion, supporting our hypothesis that CD36 functions as a protective fatty acid sensor in the liver. In addition to the reduction of PGs, we showed that the hepatic level of 20-HETE was also decreased in the CD36Tg mice without affecting the level of the parent arachidonic acid. The decreased formation of 20-HETE may have also contributed to the overall improvement of metabolic function, because this arachidonic acid metabolite has been shown to induce hyperglycemia (39).

In summary, we have uncovered a novel function of CD36 in regulating glycogen homeostasis and fasting hypoglycemia, although the mechanism by which CD36 affects glycogen homeostasis has yet to be clearly defined. Overexpression of CD36 in the liver conferred resistance to fasting hypoglycemia and metabolic harm caused by HFD feeding. We propose that CD36 serves as a protective fatty acid sensor in the liver. Rather than being a causative factor of steatosis, the induction of CD36 under HFD feeding or obesity may represent a protective response against metabolic stress and lipid overload. Manipulation of the expression or activity of hepatic CD36 may represent a novel approach to managing metabolic syndrome.

ACKNOWLEDGMENTS

We declare that no conflict of interest exists.

W. G. Garbacz, N. S. Eyre, G. Mayrhofer, and W. Xie participated in research design. W. G. Garbacz, P. Lu, T. M. Miller, N. S. Eyre, M. Xu, and S. Ren conducted experiments. W. G. Garbacz, S. M. Poloyac, and W. Xie performed data analysis. W. G. Garbacz, S. M. Poloyac, N. S. Eyre, G. Mayrhofer, and W. Xie wrote or contributed to writing the manuscript. W. Xie acquired funding.

The study was supported in part by NIH grants DK083952 and DK099232.

FUNDING INFORMATION

This work, including the efforts of Wen Xie, was funded by HHS | National Institutes of Health (NIH) (DK083952). This work, including the efforts of Wen Xie, was funded by HHS | National Institutes of Health (NIH) (DK099232).

REFERENCES

1. **Stefan N, Kantartzis K, Haring HU.** 2008. Causes and metabolic consequences of fatty liver. Endocr Rev **29:**939–960. http://dx.doi.org/10.1210/er.2008-0009.
2. **Lu B, Bridges D, Yang Y, Fisher K, Cheng A, Chang L, Meng ZX, Lin JD, Downes M, Yu RT, Liddle C, Evans RM, Saltiel AR.** 2014. Metabolic crosstalk: molecular links between glycogen and lipid metabolism in obesity. Diabetes **63:**2935–2948. http://dx.doi.org/10.2337/db13-1531.
3. **Koonen DP, Jacobs RL, Febbraio M, Young ME, Soltys CL, Ong H, Vance DE, Dyck JR.** 2007. Increased hepatic CD36 expression contributes to dyslipidemia associated with diet-induced obesity. Diabetes **56:**2863–2871. http://dx.doi.org/10.2337/db07-0907.
4. **Lee JH, Wada T, Febbraio M, He J, Matsubara T, Lee MJ, Gonzalez FJ, Xie W.** 2010. A novel role for the dioxin receptor in fatty acid metabolism and hepatic steatosis. Gastroenterology **139:**653–663. http://dx.doi.org/10.1053/j.gastro.2010.03.033.

5. **Sheedfar F, Sung MM, Aparicio-Vergara M, Kloosterhuis NJ, Miquilena-Colina ME, Vargas-Castrillon J, Febbraio M, Jacobs RL, de Bruin A, Vinciguerra M, Garcia-Monzon C, Hofker MH, Dyck JR, Koonen DP.** 2014. Increased hepatic CD36 expression with age is associated with enhanced susceptibility to nonalcoholic fatty liver disease. Aging **6:**281–295. http://dx.doi.org/10.18632/aging.100652.
6. **Zhou J, Febbraio M, Wada T, Zhai Y, Kuruba R, He J, Lee JH, Khadem S, Ren S, Li S, Silverstein RL, Xie W.** 2008. Hepatic fatty acid transporter Cd36 is a common target of LXR, PXR, and PPARgamma in promoting steatosis. Gastroenterology **134:**556–567. http://dx.doi.org/10.1053/j.gastro.2007.11.037.
7. **Buque X, Cano A, Miquilena-Colina ME, Garcia-Monzon C, Ochoa B, Aspichueta P.** 2012. High insulin levels are required for FAT/CD36 plasma membrane translocation and enhanced fatty acid uptake in obese Zucker rat hepatocytes. Am J Physiol Endocrinol Metab **303:**E504–E514. http://dx.doi.org/10.1152/ajpendo.00653.2011.
8. **Miquilena-Colina ME, Lima-Cabello E, Sanchez-Campos S, Garcia-Mediavilla MV, Fernandez-Bermejo M, Lozano-Rodriguez T, Vargas-Castrillon J, Buque X, Ochoa B, Aspichueta P, Gonzalez-Gallego J, Garcia-Monzon C.** 2011. Hepatic fatty acid translocase CD36 upregulation is associated with insulin resistance, hyperinsulinaemia and increased steatosis in non-alcoholic steatohepatitis and chronic hepatitis C. Gut **60:**1394–1402. http://dx.doi.org/10.1136/gut.2010.222844.
9. **Zhang YL, Hernandez-Ono A, Siri P, Weisberg S, Conlon D, Graham MJ, Crooke RM, Huang LS, Ginsberg HN.** 2006. Aberrant hepatic expression of PPARgamma2 stimulates hepatic lipogenesis in a mouse model of obesity, insulin resistance, dyslipidemia, and hepatic steatosis. J Biol Chem **281:**37603–37615. http://dx.doi.org/10.1074/jbc.M604709200.
10. **Nassir F, Adewole OL, Brunt EM, Abumrad NA.** 2013. CD36 deletion reduces VLDL secretion, modulates liver prostaglandins, and exacerbates hepatic steatosis in ob/ob mice. J Lipid Res **54:**2988–2997. http://dx.doi.org/10.1194/jlr.M037812.
11. **Deng B, Sullivan MA, Li J, Tan X, Zhu C, Schulz BL, Gilbert RG.** 2015. Molecular structure of glycogen in diabetic liver. Glycoconj J **32:**113–118. http://dx.doi.org/10.1007/s10719-015-9578-6.
12. **Ferrannini E, Lanfranchi A, Rohner-Jeanrenaud F, Manfredini G, Van de Werve G.** 1990. Influence of long-term diabetes on liver glycogen metabolism in the rat. Metabolism **39:**1082–1088. http://dx.doi.org/10.1016/0026-0495(90)90170-H.
13. **Krssak M, Brehm A, Bernroider E, Anderwald C, Nowotny P, Dalla Man C, Cobelli C, Cline GW, Shulman GI, Waldhausl W, Roden M.** 2004. Alterations in postprandial hepatic glycogen metabolism in type 2 diabetes. Diabetes **53:**3048–3056. http://dx.doi.org/10.2337/diabetes.53.12.3048.
14. **von Wilamowitz-Moellendorff A, Hunter RW, Garcia-Rocha M, Kang L, Lopez-Soldado I, Lantier L, Patel K, Peggie MW, Martinez-Pons C, Voss M, Calbo J, Cohen PT, Wasserman DH, Guinovart JJ, Sakamoto K.** 2013. Glucose-6-phosphate-mediated activation of liver glycogen synthase plays a key role in hepatic glycogen synthesis. Diabetes **62:**4070–4082. http://dx.doi.org/10.2337/db13-0880.
15. **Zhang Y, Xu D, Huang H, Chen S, Wang L, Zhu L, Jiang X, Ruan X, Luo X, Cao P, Liu W, Pan Y, Wang Z, Chen Y.** 2014. Regulation of glucose homeostasis and lipid metabolism by PPP1R3G-mediated hepatic glycogenesis. Mol Endocrinol **28:**116–126. http://dx.doi.org/10.1210/me.2013-1268.
16. **Puschel GP, Kirchner C, Schroder A, Jungermann K.** 1993. Glycogenolytic and antiglycogenolytic prostaglandin E2 actions in rat hepatocytes are mediated via different signalling pathways. Eur J Biochem **218:**1083–1089. http://dx.doi.org/10.1111/j.1432-1033.1993.tb18468.x.
17. **Julian MT, Alonso N, Ojanguren I, Pizarro E, Ballestar E, Puig-Domingo M.** 2015. Hepatic glycogenosis: an underdiagnosed complication of diabetes mellitus? World J Diabetes **6:**321–325. http://dx.doi.org/10.4239/wjd.v6.i2.321.
18. **Taylor AJ, Ye JM, Schmitz-Peiffer C.** 2006. Inhibition of glycogen synthesis by increased lipid availability is associated with subcellular redistribution of glycogen synthase. J Endocrinol **188:**11–23. http://dx.doi.org/10.1677/joe.1.06381.
19. **Lopez-Soldado I, Zafra D, Duran J, Adrover A, Calbo J, Guinovart JJ.** 2015. Liver glycogen reduces food intake and attenuates obesity in a high-fat diet-fed mouse model. Diabetes **64:**796–807. http://dx.doi.org/10.2337/db14-0728.
20. **O'Doherty RM, Jensen PB, Anderson P, Jones JG, Berman HK, Kearney D, Newgard CB.** 2000. Activation of direct and indirect pathways of glycogen synthesis by hepatic overexpression of protein targeting to glycogen. J Clin Invest **105:**479–488. http://dx.doi.org/10.1172/JCI8673.
21. **Zhou J, Zhai Y, Mu Y, Gong H, Uppal H, Toma D, Ren S, Evans RM, Xie W.** 2006. A novel pregnane X receptor-mediated and sterol regulatory element-binding protein-independent lipogenic pathway. J Biol Chem **281:**15013–15020. http://dx.doi.org/10.1074/jbc.M511116200.
22. **Lu P, Yan J, Liu K, Garbacz WG, Wang P, Xu M, Ma X, Xie W.** 2015. Activation of aryl hydrocarbon receptor dissociates fatty liver from insulin resistance by inducing fibroblast growth factor 21. Hepatology **61:**1908–1919. http://dx.doi.org/10.1002/hep.27719.
23. **Jiang M, He J, Kucera H, Gaikwad NW, Zhang B, Xu M, O'Doherty RM, Selcer KW, Xie W.** 2014. Hepatic overexpression of steroid sulfatase ameliorates mouse models of obesity and type 2 diabetes through sex-specific mechanisms. J Biol Chem **289:**8086–8097. http://dx.doi.org/10.1074/jbc.M113.535914.
24. **Folch J, Lees M, Sloane Stanley GH.** 1957. A simple method for the isolation and purification of total lipids from animal tissues. J Biol Chem **226:**497–509.
25. **Poloyac SM, Zhang Y, Bies RR, Kochanek PM, Graham SH.** 2006. Protective effect of the 20-HETE inhibitor HET0016 on brain damage after temporary focal ischemia. J Cereb Blood Flow Metab **26:**1551–1561. http://dx.doi.org/10.1038/sj.jcbfm.9600309.
26. **Theken KN, Deng Y, Schuck RN, Oni-Orisan A, Miller TM, Kannon MA, Poloyac SM, Lee CR.** 2012. Enalapril reverses high-fat diet-induced alterations in cytochrome P450-mediated eicosanoid metabolism. Am J Physiol Endocrinol Metab **302:**E500–E509. http://dx.doi.org/10.1152/ajpendo.00370.2011.
27. **Parniak MA, Kalant N.** 1988. Enhancement of glycogen concentrations in primary cultures of rat hepatocytes exposed to glucose and fructose. Biochem J **251:**795–802. http://dx.doi.org/10.1042/bj2510795.
28. **Lo S, Russell JC, Taylor AW.** 1970. Determination of glycogen in small tissue samples. J Appl Physiol **28:**234–236.
29. **Mustonen AM, Kakela R, Halonen T, Karja V, Vartiainen E, Nieminen P.** 2012. Fatty acid mobilization in voles: model species for rapid fasting response and fatty liver. Comp Biochem Physiol A Mol Integr Physiol **163:**152–160. http://dx.doi.org/10.1016/j.cbpa.2012.05.196.
30. **Wapnir RA, Lifshitz F.** 1977. Fasting-induced hypoglycemia in experimentally malnourished rats. J Nutr **107:**383–390.
31. **Magnusson I, Rothman DL, Jucker B, Cline GW, Shulman RG, Shulman GI.** 1994. Liver glycogen turnover in fed and fasted humans. Am J Physiol **266:**E796–E803.
32. **Cohen P, Nimmo HG, Proud CG.** 1978. How does insulin stimulate glycogen synthesis? Biochem Soc Symp **43:**69–95.
33. **Nuttall FQ, Gilboe DP, Gannon MC, Niewoehner CB, Tan AW.** 1988. Regulation of glycogen synthesis in the liver. Am J Med **85:**77–85. http://dx.doi.org/10.1016/0002-9343(88)90400-7.
34. **Viollet B, Horman S, Leclerc J, Lantier L, Foretz M, Billaud M, Giri S, Andreelli F.** 2010. AMPK inhibition in health and disease. Crit Rev Biochem Mol Biol **45:**276–295. http://dx.doi.org/10.3109/10409238.2010.488215.
35. **Cohen PT.** 2002. Protein phosphatase 1: targeted in many directions. J Cell Sci **115:**241–256.
36. **Korrodi-Gregorio L, Esteves SL, Fardilha M.** 2014. Protein phosphatase 1 catalytic isoforms: specificity toward interacting proteins. Transl Res **164:**366–391. http://dx.doi.org/10.1016/j.trsl.2014.07.001.
37. **Kuda O, Jenkins CM, Skinner JR, Moon SH, Su X, Gross RW, Abumrad NA.** 2011. CD36 protein is involved in store-operated calcium flux, phospholipase A2 activation, and production of prostaglandin E2. J Biol Chem **286:**17785–17795. http://dx.doi.org/10.1074/jbc.M111.232975.
38. **Nauli AM, Nassir F, Zheng S, Yang Q, Lo CM, Vonlehmden SB, Lee D, Jandacek RJ, Abumrad NA, Tso P.** 2006. CD36 is important for chylomicron formation and secretion and may mediate cholesterol uptake in the proximal intestine. Gastroenterology **131:**1197–1207. http://dx.doi.org/10.1053/j.gastro.2006.08.012.
39. **Lai G, Wu J, Liu X, Zhao Y.** 2012. 20-HETE induces hyperglycemia through the cAMP/PKA-PhK-GP pathway. Mol Endocrinol **26:**1907–1916. http://dx.doi.org/10.1210/me.2012-1139.
40. **Sacerdoti D, Balazy M, Angeli P, Gatta A, McGiff JC.** 1997. Eicosanoid excretion in hepatic cirrhosis. Predominance of 20-HETE. J Clin Invest **100:**1264–1270. http://dx.doi.org/10.1172/JCI119640.
41. **Silverstein RL, Febbraio M.** 2009. CD36, a scavenger receptor involved in immunity, metabolism, angiogenesis, and behavior. Sci Signal **2:**re3. http://dx.doi.org/10.1126/scisignal.272re3.
42. **Wilson CG, Tran JL, Erion DM, Vera NB, Febbraio M, Weiss EJ.** 2016.

Hepatocyte-specific disruption of CD36 attenuates fatty liver and improves insulin sensitivity in HFD-fed mice. Endocrinology **157:**570–585. http://dx.doi.org/10.1210/en.2015-1866.

43. **Macauley M, Smith FE, Thelwall PE, Hollingsworth KG, Taylor R.** 2015. Diurnal variation in skeletal muscle and liver glycogen in humans with normal health and type 2 diabetes. Clin Sci **128:**707–713. http://dx.doi.org/10.1042/CS20140681.
44. **Ros S, Garcia-Rocha M, Calbo J, Guinovart JJ.** 2011. Restoration of hepatic glycogen deposition reduces hyperglycaemia, hyperphagia and gluconeogenic enzymes in a streptozotocin-induced model of diabetes in rats. Diabetologia **54:**2639–2648. http://dx.doi.org/10.1007/s00125-011-2238-x.
45. **Rui L.** 2014. Energy metabolism in the liver. Compr Physiol **4:**177–197. http://dx.doi.org/10.1002/cphy.c130024.
46. **Luo X, Zhang Y, Ruan X, Jiang X, Zhu L, Wang X, Ding Q, Liu W, Pan Y, Wang Z, Chen Y.** 2011. Fasting-induced protein phosphatase 1 regulatory subunit contributes to postprandial blood glucose homeostasis via regulation of hepatic glycogenesis. Diabetes **60:**1435–1445. http://dx.doi.org/10.2337/db10-1663.
47. **Gomez-Foix AM, Rodriguez-Gil JE, Guinovart JJ, Bosch F.** 1989. Prostaglandins E2 and F2 alpha affect glycogen synthase and phosphorylase in isolated hepatocytes. Biochem J **261:**93–97. http://dx.doi.org/10.1042/bj2610093.
48. **de Souza HM, Borba-Murad GR, Ceddia RB, Curi R, Vardanega-Peicher M, Bazotte RB.** 2001. Rat liver responsiveness to gluconeogenic substrates during insulin-induced hypoglycemia. Braz J Med Biol Res **34:**771–777. http://dx.doi.org/10.1590/S0100-879X2001000600012.
49. **Newgard CB, Hirsch LJ, Foster DW, McGarry JD.** 1983. Studies on the mechanism by which exogenous glucose is converted into liver glycogen in the rat. A direct or an indirect pathway? J Biol Chem **258:**8046–8052.
50. **Bjornsson OG, Sparks JD, Sparks CE, Gibbons GF.** 1992. Prostaglandins suppress VLDL secretion in primary rat hepatocyte cultures: relationships to hepatic calcium metabolism. J Lipid Res **33:**1017–1027.
51. **Okumura T, Kanemaki T, Kitade H.** 1993. Stimulation of glucose incorporation into glycogen by E-series prostaglandins in cultured rat hepatocytes. Biochim Biophys Acta **1176:**137–142.